The Albedo of Junipers

Measured in Summer 2009 at the Niederhorn, Switzerland

Werner Eugster[1,*] and Brigitta Ammann[2]

[1] ETH Zürich, Institute of Plant Sciences, CH–8092 Zürich, Switzerland
[2] University of Bern, Oeschger Centre, CH–3012 Bern, Switzerland

January 24, 2012

1 Introduction

This field study was performed to obtain a defensible value for the surface reflectivity (albedo) of *Juniper* shrublands that could be used by Brigitta Ammann to quantitatively assess the role of *Juniper* shrublands in surface energy balance feedbacks to climate after the last glaciation.

2 Methods

2.1 Field Site

Field measurements were carried out over *Juniperus communis* L. ssp. *alpina* (NEILR.) ČELAK. shrubs at the Niederhorn, Beatenberg, Switzerland. The locality is approximately 300 m to the SE of the mountain top at an elevation of 1920 m a.s.l. (Figure 1).

2.2 Instrument and Data Aquisition

For this project we used a Kipp and Zonen (Delft, The Netherlands) CNR-1 net radiometer, an instrument consisting of two pairs of upward and downward looking sensors. We used the instru-

*Correspondence to: Werner Eugster, ETH Zürich, Institute of Plant Sciences, LFW C55.2, CH–8092 Zürich, Switzerland. E-mail werner.eugster@usys.ethz.ch, fax +41 44 632 1153.

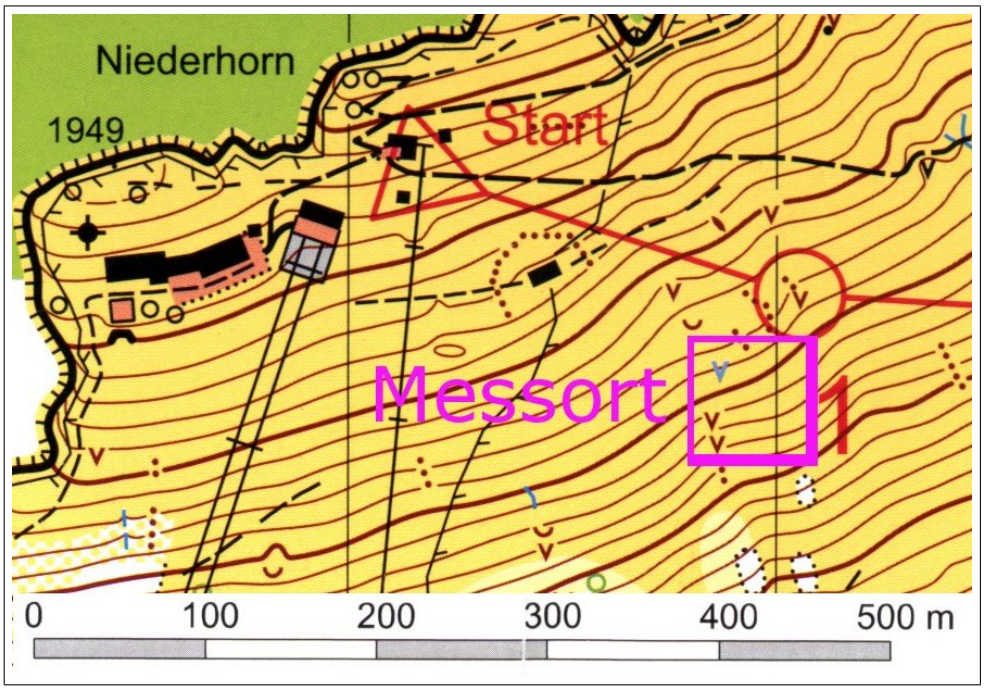

Figure 1: Locality of field site on orienteering map of the Niederhorn slope. Contour lines are drawn at 5 m intervals. Map copyright owner: OLG Thun.

ment with serial number 980077 (property of University of Bern) with a nominal sensor sensitivity of $10.04 \cdot 10^{-6}$ V per W m^{-2}.

Each pair of sensor is either a pyranometer or a pyrgeometer of the same type. Pyranometers (Kipp and Zonen, model CM-3) measure short-wave radiation, whereas pyrgeometers (Kipp and Zonen, model CG-3) measure thermal infrared radiation.

The manual specifies the sensitivy range to be 305–2800 nm (Figure 3) for the pyranometers with a $\pm$ 5% spectral selectivity in the range 350–1500 nm, and a non-linearity of $\pm$ 2.5% (0–1000 W m^{-2}). The temperature sensitivity is specified to be $\pm$ 6% in the temperature range –10 to +40°C.

The pyrgeometers are not directly used to determine albedo, but they allow to back-calculate long-wave surface radiation flux and thus surface temperature. This is helpful to detect periods with snow

Figure 2: Locality of field site on satellite images of the Niederhorn slope. Copyright: Teleatlas/Mapsearch.ch.

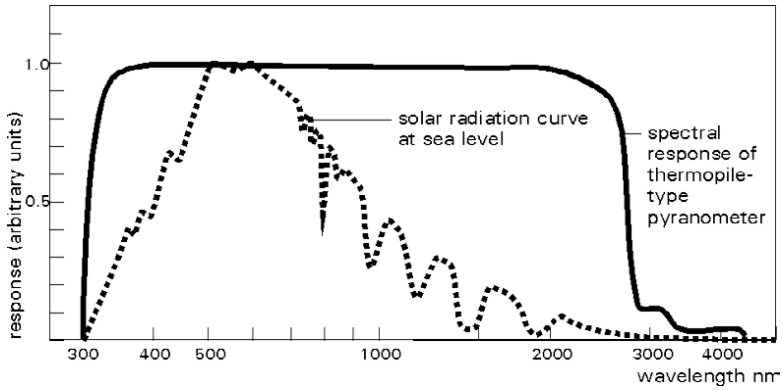

Figure 3: Spectral characteristics of the Kipp & Zonen CM-3 pyranometers used in the CNR1 net radiometer. The spectral sensitivity relates to clear sky conditions. From Kipp & Zonen CNR1 manual.

cover during our experiment. The Kipp & Zonen manual indicates a transmissivity window in the far infrared range 4–40 μm (Figure 5; exact values are not given in the Kipp & Zonen manual).

The instrument temperature was measured with the built-in Pt100 platinum resistor sensor using a 4-wire full bridge measurement setup. All measurements were done with a Campbell Scientific data logger, model CR10X. Measurements were done every 10 seconds, and stored as 5 minute averages.

2.3 Sensor Calibration

Rebecca Hiller carried out an intercalibration at the World Radiation Center in Davos in late 2006. See Table 3.4 in her diploma thesis (Hiller 2007). Her correction is based on the factory calibration, that is modified in the following way:

$$K_{in} = 5.55 + 1.02\,x \quad (1)$$

$$K_{out} = 6.04 + 1.05\,x \quad (2)$$

$$T_{CNR1} = 29.55 + 0.88\,x \quad (3)$$

Long-wave radiation measurements were only corrected for the temperature offset since the sensors measure the difference between the radiation temperature of the instrument body and the sensor surface.

2.4 Albedo Calculations

Albedo α is defined as

$$\alpha = \frac{K_{out}}{K_{in}}\ . \quad (4)$$

Thus, inaccuracies in the measurement of the long-wave radiation and the instrument body temperature have no effect on the albedo.

Albedo values are either reported as rations (in the range 0–1) or as percentages (range 0%–100%). Here we use ratios to avoid the confusion that always is created when percent change of a percentage is used. With ratios no such confusion should arise.

Figure 4: The instrument (Kipp & Zonen CNR1 Net Radiometer) at its measurement position over the Juniper shrub area. Albedo was measured with the two sensors having a transparent quartz glass dome (one sensor looking upwards, the other downwards). The two sensors with a flat dark filter glass are the pyrgeometers for long-wave radiation measurements.

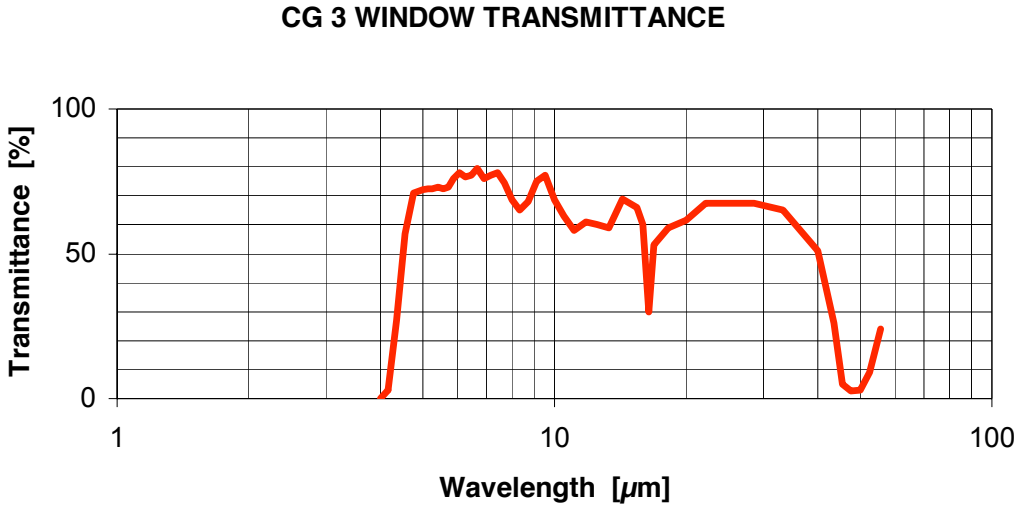

Figure 5: Spectral characteristics of the Kipp & Zonen CG-3 pyrgeometers used in the CNR1 net radiometer. From Kipp & Zonen CNR1 manual.

3 Results

Figures 6–8 show the original raw data of the full measurement period.

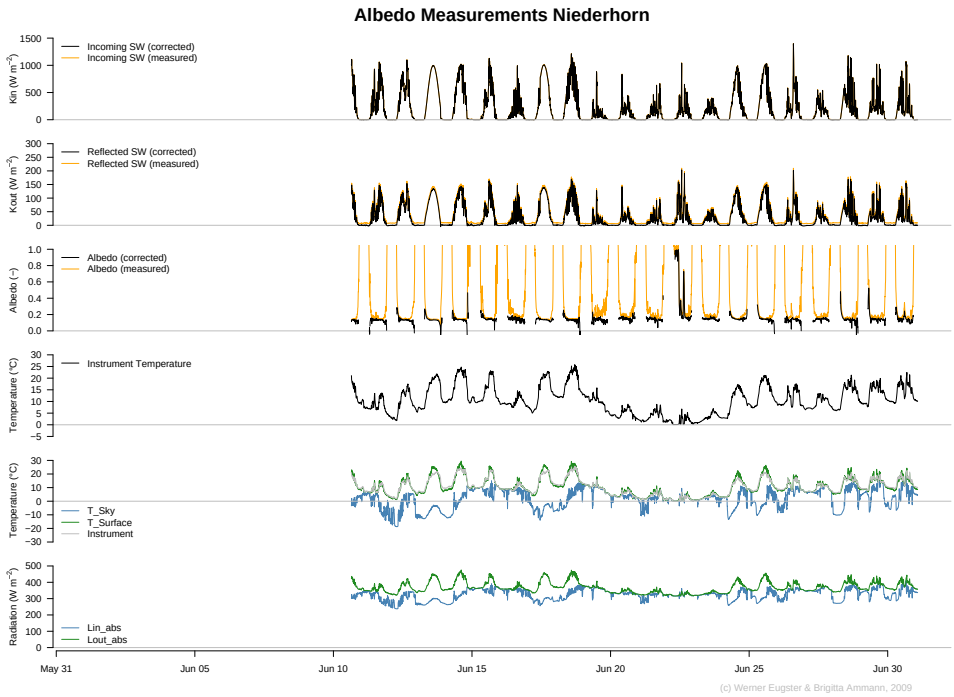

Figure 6: Example of raw data (5-minute resolution) for June 2009.

There are always 6 panels. To correct for the temperature sensitivity of the pyranometers, which are mostly influencing the offset value of the absolute measurements, we show both the measured and corrected values in the top panels. The color coding is that the orange lines are the raw measured values (which include the calibration correction as specified in the Methods section), whereas the black lines are the corrected values used for the calculation of the albedo.

The offset correction is done as follows. Since by definition there is no short-wave radiation at night, we determined the mean radiation measured during the night for each 24-hour period. This value should correspond to 0 W m^{-2}. All values were then shifted by the respective offset to achieve a nocturnal mean of 0 W m^{-2}. In Figure 6 for example it is quite clear that the offset for incoming radiation (top panel) was very small, and thus the orange line is hidden behind the black line. In the case of the reflected shortwave radiation the nocturnal values were positive, and thus a correction moved down the curve to yield 0 W m^{-2} at night.

The third panel shows the influence of this correction on the albedo calculation with Eq. (4). However, in addition to the correction described so far, the black curves only show albedo values that meet the following conditions: (1) short-wave incoming radiation $K_{in} \geq 10$ W m^{-2}; (2) $K_{out} < K_{in}$; and (3) $K_{out} > 0$ W m^{-2}. The last points removes some artefacts where reflections from e.g. the lake or a glass window on a building may accidentally reflect solar radiation to the downward looking sensor. Since albedo is a ratio, the denominator must be larger than the accuracy of the CM-3 sensor. Since the CM-3 are secondary class radiation sensors, the overall accuracy despite all corrections should not be expected to be better than 10 W m^{-2}, thus this threshold for rejecting albedo values.

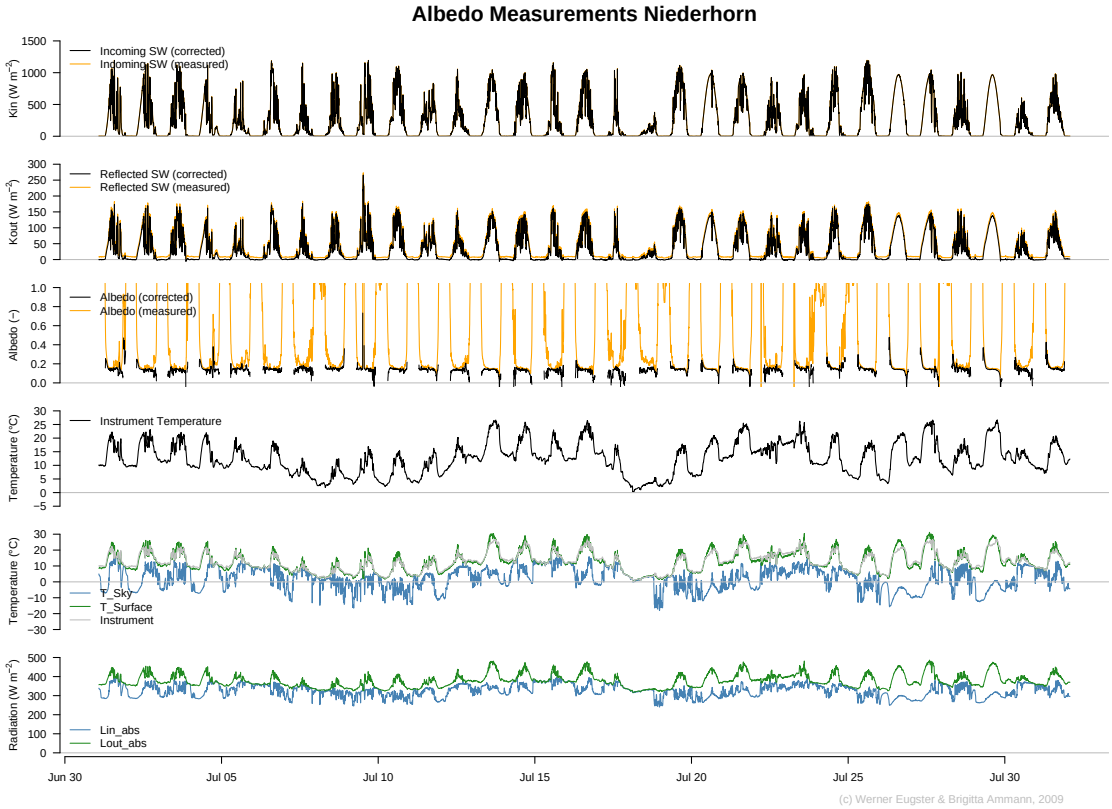

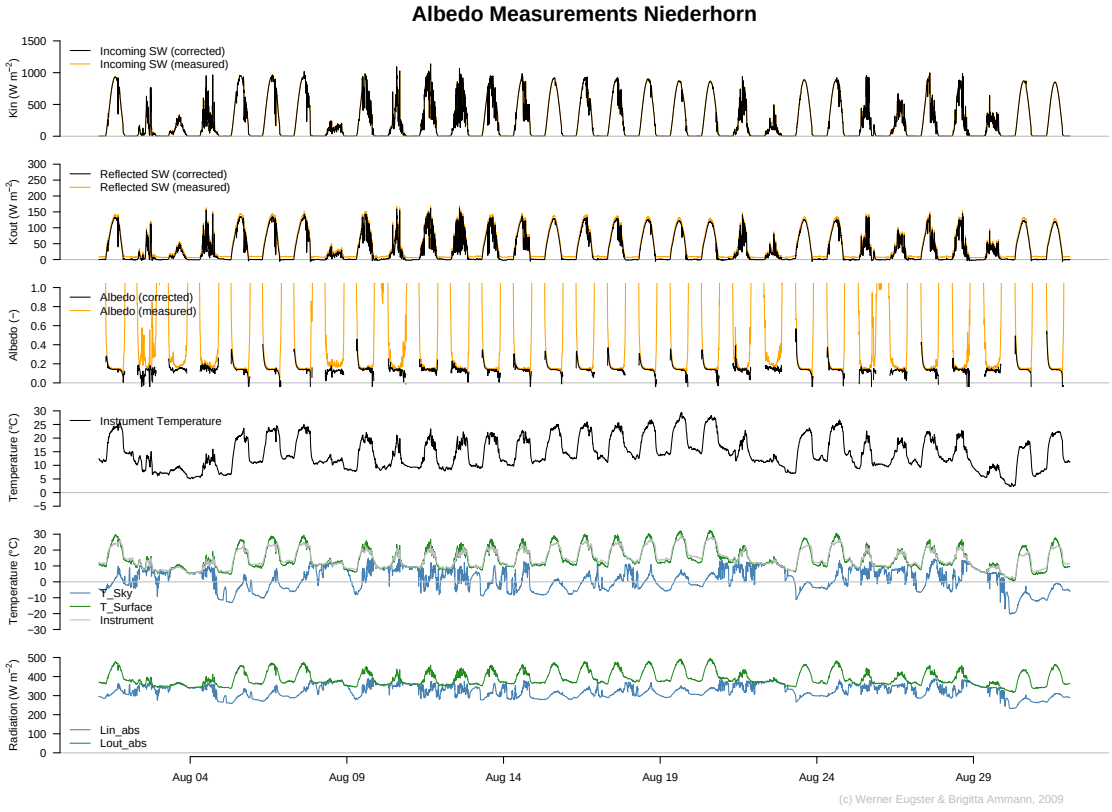

Figure 7: Example of raw data (5-minute resolution) for July and August 2009.

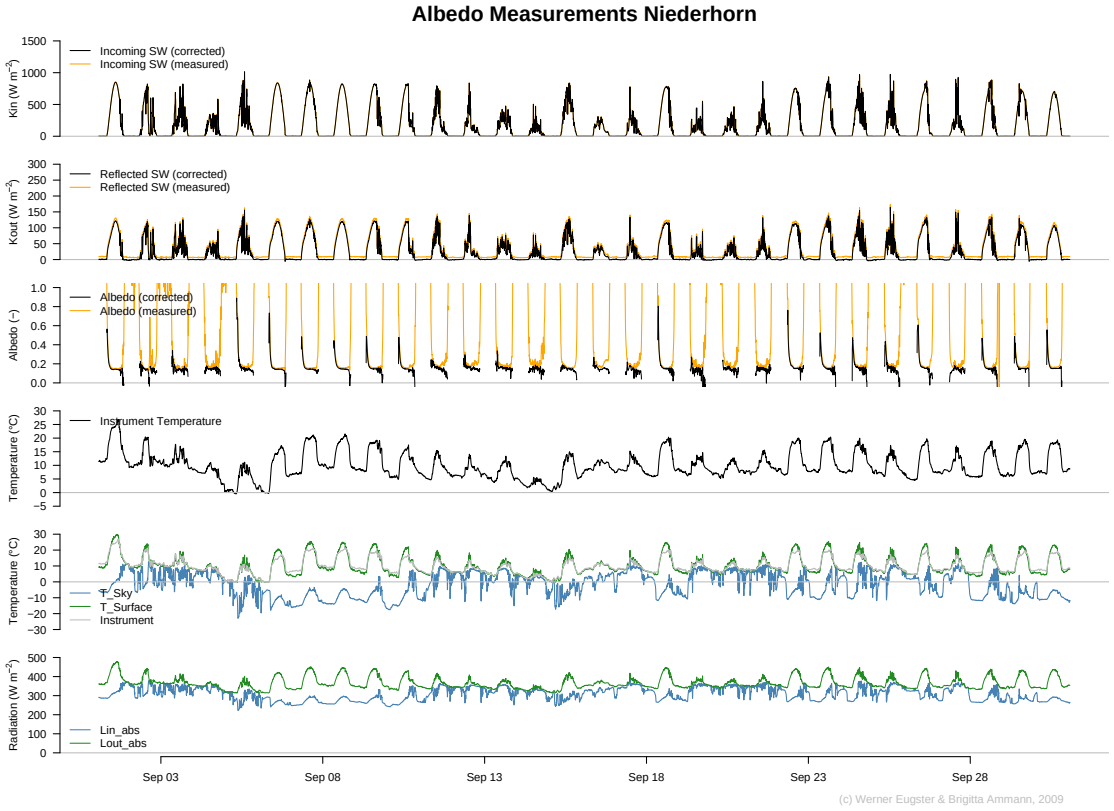

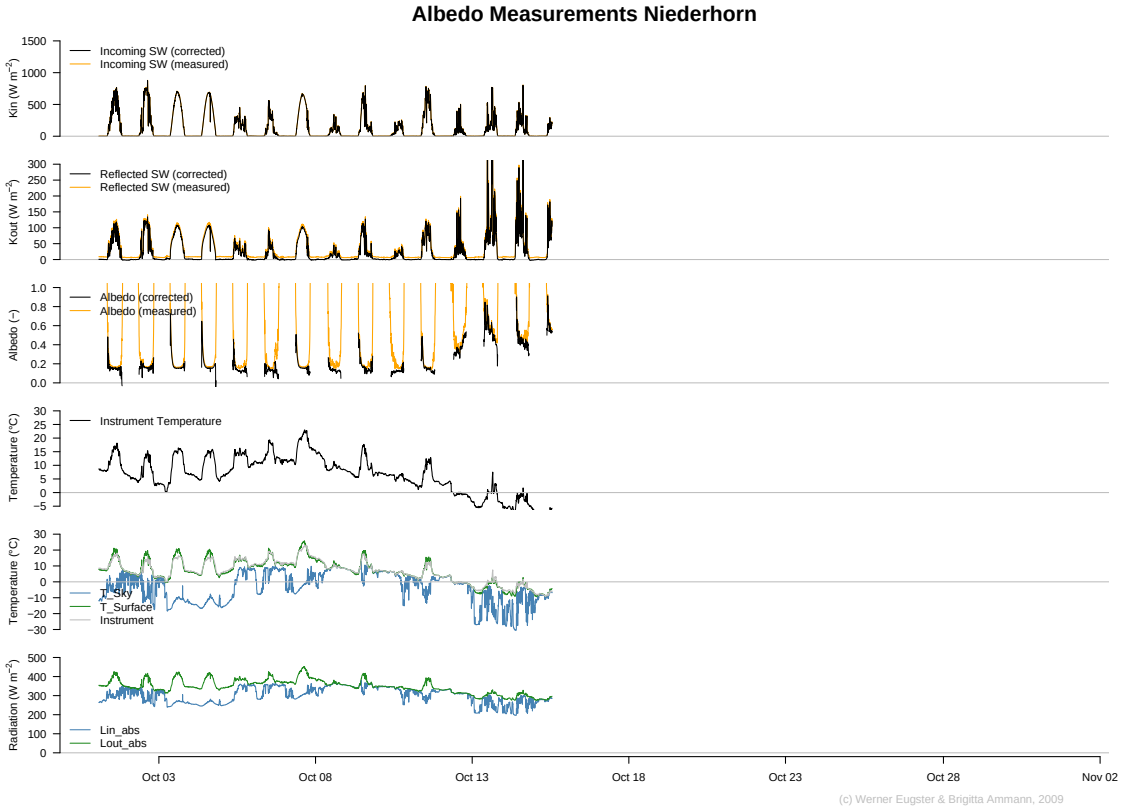

Figure 8: Example of raw data (5-minute resolution) for September and October 2009.

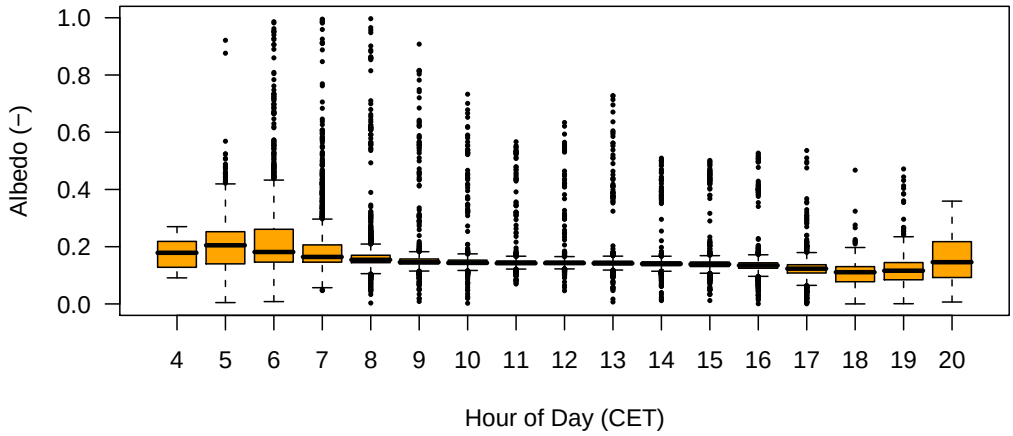

Figure 9: Diurnal cycle of albedo for conditions with K_{in} >10 W m^{-2} and K_{out} >0 W m^{-2}. Boxplots showing median (horizontal solid line), inter-quartile range (orange box), whiskers and outliers.

3.1 Diurnal Cycle of Albedo

Albedo values are not always reported very consistently. Normally, there is a diurnal cycle in albedo which is driven by (a) solar elevation angle, (b) the changing ratio of diffuse vs. direct radiation over the diurnal course, (c) due to possible active response of vegetation to the position of the sun, and maybe others. I have not made any literature research on this, thus this list may be incomplete.

a. Solar elevation angle. Typically, the reflectivity on a solid surface depends on the angle between the incoming radiation and the surface. Thus, the effect of solar elevation angle on daily and seasonal time scale are relevant questions that need to be addressed to be able to understand the effect of changes in albedo on the surface energy budget.

b. Changing ratio of diffuse vs. direct radiation. Typically, there is less absolute humidity in the air in the morning than in the afternoon. The main reason is that the air cools during the night, and if it cools down to the temperature where 100% relative humidity is reached, then dew may form at the surface. When the atmosphere heats up, the moisture is preserved in the air (although relative humidity goes down as temperature goes up), and daily evapotranspiration from vegetation and other surfaces increase the overall atmospheric moisture beyond the level that was found early in the morning. Since a higher absolute humidity means more scatter of direct sunlight, there is a shift towards a higher share of diffuse vs. direct light over the diurnal course.

Since diffuse light can penetrate deeper into a plant canopy than direct light, the albedo tends to decrease as the fraction of diffuse vs. direct light increases. In summary, there is a minimum daily albedo in typical diurnal cycles. In remote sensing and modeling literature, it is mostly this daily minimum albedo that is used, because averaging a ratio such as the albedo is meaningless and does not help the case. However, many publications do not mention whether they report on instantaneous values (which can give a strong experimental bias) or carefully derived mean daily minimum albedo values.

c. Active response of vegetation to position of sun. Besides these physical effects, some plants adjust their leaf position with respect to the position of the sun. Hence, the reflectivity may also change on whether the leaves are facing the sun or whether they are at an angle that reflects more sunlight.

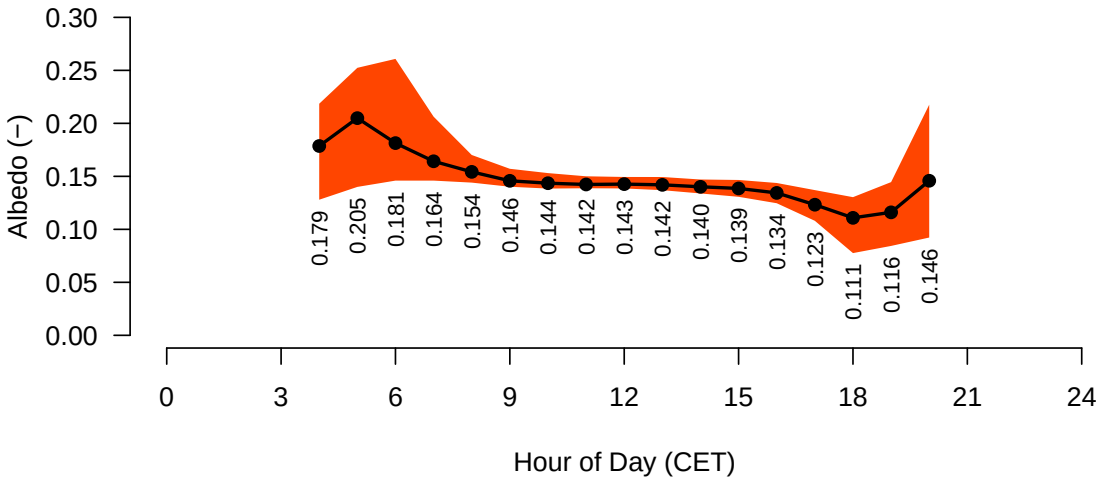

Figure 10: Same as in Figure 9, but only showing the inter-quartile range of hourly grouped data (orange area) and the median values for each hour (circles). The values printed below each symbol give the median albedo for the respective hour of day.

Figure 9 shows boxplots (McGill et al. 1978) with all selected albedo values, grouped by hour of day. To extract average conditions it is convenient to only extract the inter-quartile range and median values from such boxplots. This is done in Figure 10.

Figure 10 gives the median hourly albedo and the inter-quartile range of all accepted albedo measurements. Thus, such a plot by definition uses the 50% of all values that are in the center of the empirical probability distribution of values. These values most likely are best suited to extract general conditions, ignoring high albedo values due to fresh snow or artificially low albedo due to reflections from objects below the downward looking sensor. This artefact is of particular importance since we measured on a mountain slope more than 1000 m above the lake and inhabited areas where reflections (glass windows) and other disturbances may be the cause for outliers.

Figure 10 shows the typical diurnal course, except for the fact that the lowest values are found around 18 hours CET. This may well be an artifact of the locality. During the late afternoon hours, the sun is well visible during summer, but may cause reflections on the lake that are not automatically removed even by such statistical selection.

For the purpose of quantifying the albedo for *Juniper* it is thus probably best to specify noontime albedo which is **0.143**.

Since the albedo values do not change strongly during noontime (which is around 12:30 CET), we also can derive a best estimate from the time period 10–15 hours CET (to be precise: with our 5-minute averages this means that we consider all measurements obtained between 09:55 CET and 14:55 CET). In Figure 11 these values are shown in the top panels. They are not really normally distributed, as the Q-Q plot shows. Thus, we further restricted the selection to the range with quasi-normal distribution, that is, we eliminated values with albedo <0.08 or >0.20. With this additional criterion we obtain a data subset that is still not perfectly normally distributed, but it is a symmetric distribution and thus allows the parameterization with an arithmetic mean and standard deviation. It is not surprising that the albedo is not normally distributed since it is a ratio of two measurements.

Nevertheless, with this selection we can specify the noontime albedo to be **0.142** $\pm$ **0.024** for the 2-sigma range ($\approx$95% confidence interval).

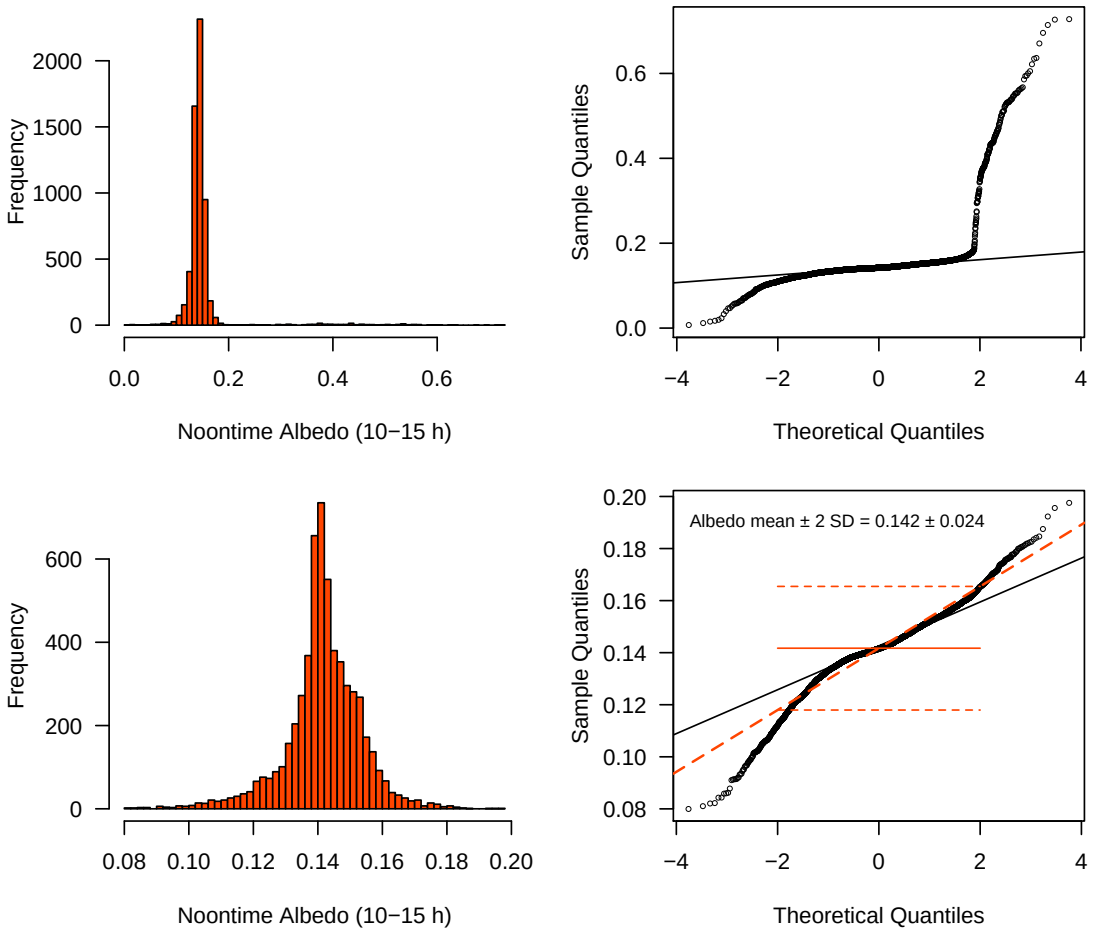

Figure 11: Noontime albedo for the time period 10–15 hours CET. Top: selection of data points with K_{in} >10 W m^{-2} and K_{out} >0 W m^{-2} (top panels) and additionally restricting the valid range to 0.08–0.2 to reduce the influence of extremes (bottom panels). Histograms are plotted at left, and Q-Q-Q plots for normal distribution are at right. The horizontal solid and dashed lines in the lower left panel show the arithmetic mean ± 2 SD.

3.2 Seasonal Trend of Albedo

The initial expectation was that there might be a seasonal change in albedo, (a) due to change in solar elevation, and/or (b) due to change in greenness of the Juniper shrubs. In June, the new shoots which are somewhat brighter green than the old shoots were present, and one could have expected a decline of albedo over the season.

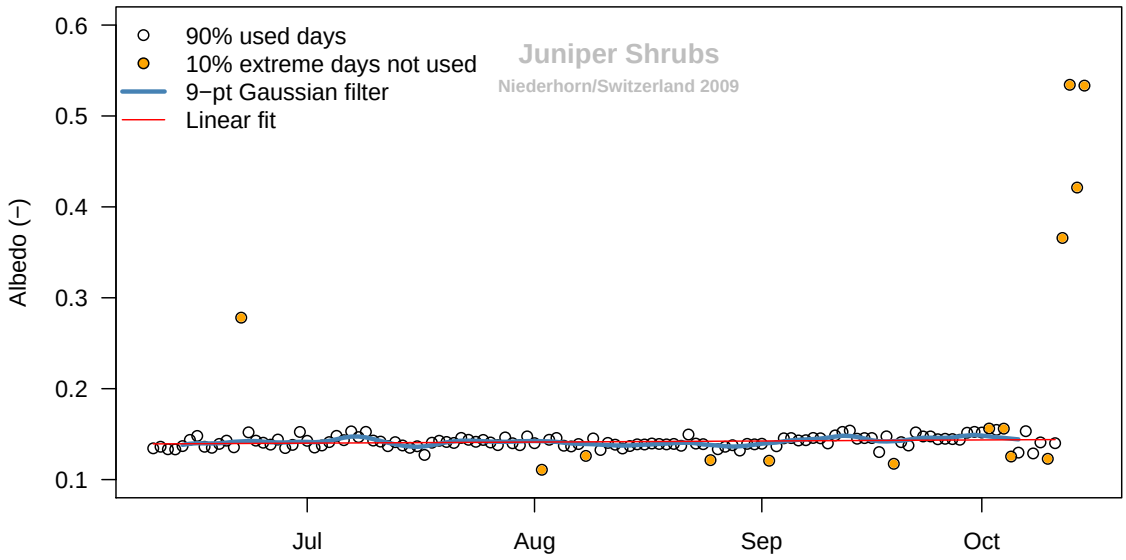

Figure 12: Daily mean albedo for 10–15 hours CET for each day. There was one short snowfall in June and over the last 4 days of measurements. The 9-point Gaussian filter and the linear fit excluded 10% of days with extreme albedo values (symmetric exclusion, 5% on both sides; orange points were excluded from fits).

Our measurements, however, document the opposite effect (Figure 12, red line): there was a slight increase of the albedo over the growing season.

```
Call:
lm(formula = Albedo.noontime$Albedo ~ Albedo.noontime$DOY, subset = use)

Residuals:
       Min         1Q     Median         3Q        Max
-0.0150863 -0.0033777 -0.0002570  0.0031047  0.0127578

Coefficients:
                     Estimate Std. Error t value Pr(>|t|)
(Intercept)         1.331e-01  3.423e-03  38.872   <2e-16 ***
Albedo.noontime$DOY 3.856e-05  1.534e-05   2.514   0.0133 *
---
Signif. codes:  0 ‘***’ 0.001 ‘**’ 0.01 ‘*’ 0.05 ‘.’ 0.1 ‘ ’ 1

Residual standard error: 0.005761 on 112 degrees of freedom
Multiple R-squared: 0.05343,Adjusted R-squared: 0.04498
F-statistic: 6.322 on 1 and 112 DF,  p-value: 0.01334
```

That is, the albedo increased by 0.00003856 $\pm$ 0.00001534 every day. That is, over the 128 days of measurements (day of year 161–288) the albedo increased by 0.0049 $\pm$ 0.0020, which is most likely a negligible seasonal evolution. It is most probably related to the decreasing solar elevation angle, which tends to increase the reflection on objects compared to high solar angles (late June).

3.3 Variability of Daily Albedo

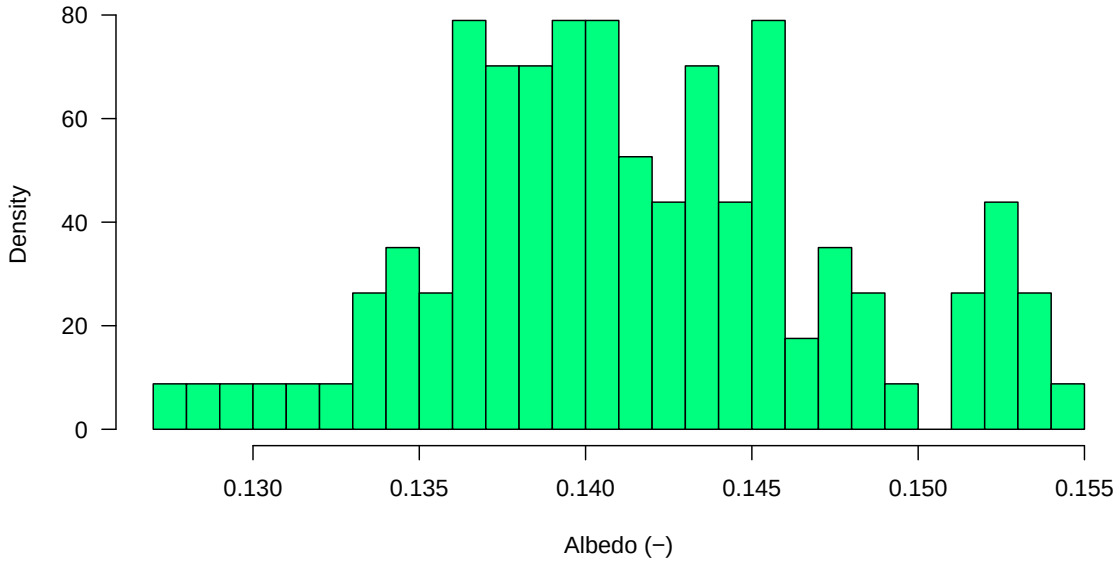

Figure 13: Histogram of daily albedo values (mean 10–15 hours CET) of the 90% days used for the fits in Figure 12.

3.4 Dependence of Albedo on Cloud Cover

3.4.1 Clear-sky conditions

Days with a mean global radiation of $\geq$250 W m^{-2} during the time period 10–15 hours CET were selected. During these conditions the albedo was 0.1391 $\pm$ 0.0029 (mean $\pm$ SD), N = 40 (Figure 14, right).

3.4.2 Partially cloudy conditions

Days with a mean global radiation of $\geq$150 W m^{-2} to $<$220 W m^{-2} during the time period 10–15 hours CET were selected. During these conditions the albedo was 0.1448 $\pm$ 0.0075 (mean $\pm$ SD), N = 34 (Figure 14, center).

3.4.3 Overcast conditions

Days with a mean global radiation of $\geq$40 W m^{-2} to $<$100 W m^{-2} during the time period 10–15 hours CET were selected. During these conditions the albedo was 0.1363 $\pm$ 0.0113 (mean $\pm$ SD), N = 23 (Figure 14, left).

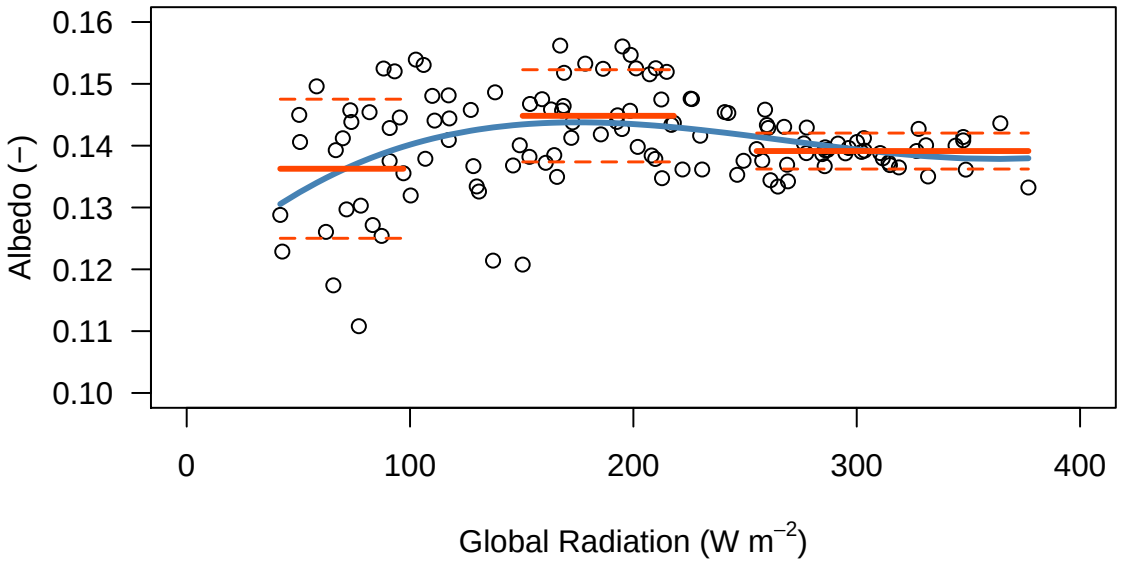

Figure 14: Albedo values depend on the fraction of diffuse light, which is higher with clouds than during clear-sky conditions. This graph plots the daily albedo (10–15 hours CET) as a function of mean global radiation (10–15 hours CET) and provides mean $\pm$ standard deviation for three conditions: clear sky; partially cloudy; overcast.

4 Conclusions

[1] During noontime the albedo values were very consistent throughout the season with a small trend towards lower values as the day progressed. Some very low values before sunset were questioned in a way that the best estimate for daytime albedo was derived from the data obtained from 10 to 15 hours CET, which yielded

$$\textbf{Noontime } \alpha = \mathbf{0.142 \pm 0.024} \qquad (\text{mean} \pm 2\ \sigma)$$

[2] The seasonal trend was quite small and could be neglected

[3] More important are the differences between clear-sky conditions, partially cloudy conditions, and overcast sky. The different albedos are

$$\textbf{Clear-sky } \alpha = \mathbf{0.139 \pm 0.006} \qquad (\text{mean} \pm 2\ \sigma)$$

$$\textbf{Partially cloudy sky } \alpha = \mathbf{0.145 \pm 0.015} \qquad (\text{mean} \pm 2\ \sigma)$$

$$\textbf{Overcast sky } \alpha = \mathbf{0.136 \pm 0.023} \qquad (\text{mean} \pm 2\ \sigma)$$

References

Hiller, R. (2007) Growing season CO_2 budget of an Alpine grassland in the Swiss Alps. Master's thesis, University of Bern, Institute of Geography. 90 pp.

McGill, R., J. W. Tukey, and W. A. Larsen (1978) Variations of box plots. *The American Statistician* **32** (1), 12–16.